



HAL
open science

Targeted assembly and synchronization of self-spinning microgears

Antoine Aubret, Mena Youssef, Stefano Sacanna, Jérémie Palacci

► **To cite this version:**

Antoine Aubret, Mena Youssef, Stefano Sacanna, Jérémie Palacci. Targeted assembly and synchronization of self-spinning microgears. *Nature Physics*, 2018, 14 (11), pp.1114-1118. 10.1038/s41567-018-0227-4 . hal-03279161

HAL Id: hal-03279161

<https://hal.science/hal-03279161>

Submitted on 6 Jul 2021

HAL is a multi-disciplinary open access archive for the deposit and dissemination of scientific research documents, whether they are published or not. The documents may come from teaching and research institutions in France or abroad, or from public or private research centers.

L'archive ouverte pluridisciplinaire **HAL**, est destinée au dépôt et à la diffusion de documents scientifiques de niveau recherche, publiés ou non, émanant des établissements d'enseignement et de recherche français ou étrangers, des laboratoires publics ou privés.

Targeted Assembly and Synchronization of Self-Spinning Microgears

Antoine Aubret¹, Mena Youssef², Stefano Sacanna², Jérémie Palacci^{1*}

¹Department of Physics, University of California, San Diego, USA

²Department of Chemistry, New York University, USA

Self-assembly is the autonomous organization of components into patterns or structures: an essential ingredient of biology and a desired route to complex organization¹. At equilibrium, the structure is encoded through specific interactions²⁻⁸, at an unfavorable entropic cost for the system. An alternative approach, widely used by Nature, uses energy input to bypass the entropy bottleneck and develop features otherwise impossible at equilibrium⁹. Dissipative building blocks that inject energy locally were made available by recent advance in colloidal science^{10,11} but have not been used to control self-assembly. Here we show the targeted formation of self-powered microgears from active particles and their autonomous synchronization into dynamical superstructures. We use a photoactive component that consumes fuel, hematite, to devise phototactic microswimmers that form self-spinning microgears following spatiotemporal light patterns. The gears are coupled *via* their chemical clouds by diffusio-phoresis¹² and constitute the elementary bricks of synchronized superstructures, which autonomously regulate their dynamics. The results are quantitatively rationalized on the basis of a stochastic description of diffusio-phoretic oscillators dynamically coupled by chemical gradients. Our findings harness non-equilibrium phoretic phenomena to program interactions and direct self-assembly with fidelity and specificity. It lays the groundwork for the autonomous construction of dynamical architectures and functional micro-machinery.

The self-assembly of complex structures which emulate the fidelity and tunability of their biological counterparts is a fundamental goal of material science and engineering. In colloidal

science, the paradigm for equilibrium self-assembly encodes information through specific interactions between building blocks that, in turn, promote assembly, so that the resulting (static) structure is the thermodynamic ground state. Emergent properties in Active Matter¹³, in which self-driven units convert an energy source into useful motion and work, have been the focus of intensive experimental and theoretical studies in recent years and primarily focused on meso-scale or macroscopic fluxes¹⁴, flocks^{15,16} or flows^{17,18} from local mechanical forcing. Their use to design nonequilibrium interactions and control self-assembly remains, however, largely unexplored^{19–22}. We introduce a sequential approach in order to architect structures, the dynamics of which arise from chemical gradients through diffusiophoretic interactions. The process is dissipative and utilizes a photocatalytic material, hematite, to harvest energy from a hydrogen peroxide fuel²³ and form hierarchical superstructures through non-equilibrium pathways (Fig.1). Instrumental to our work is the development of phototactic swimmers (Fig.1A), which direct along light gradients and assemble into self-spinning microgears or *rotors* (Fig.1B). We focus in this Letter on the self-organization of moderate numbers of rotors with manually sorted spins. They organize into stable patterns, which dynamics originates from the interplay between the phase and the space coordinates of the components. For example, sets of 7 rotors form hexagonal patterns (movie S1, Fig.1C), and exhibit an edge-current traveling at $\Omega \sim 0.1$ rad/s for co-rotating rotors (movie S2) or remain static for structures with alternating spins (movie S3). Switching off the light, the system swiftly returns to equilibrium, the interactions vanish and the order is destroyed by thermal noise (Fig.1C-inset).

A hematite cube (α -Fe₂O₃) decomposes hydrogen peroxide, at rate $\nu = \beta I / (I + I_0)$, dependent on the light intensity I ²³. It travels toward the low intensity in a gradient as a result of the asymmetric fuel consumption and diffusiophoresis¹², the migration of a colloidal particle in a concentration gradient ∇c . The measured velocity shows a good agreement with the diffusiophoretic velocity, $V \propto \nabla c \propto \nabla \nu(I)$, predicted from the experimental intensity profile (Fig.2A). The migration is slow, $V \sim 2 \mu\text{m/s}$, as the gradient on the particle scale is moderate. Following, we

devise swimmers with a fore-aft asymmetry, consisting of the extrusion of the hematite cube from a chemically inert polymer bead²⁴ (SI). In uniform light, they exhibit a persistent random walk as previously reported for Janus microswimmers^{11,25}. The polymer bead heads and the velocity, up to $30 \mu\text{m/s}$, is controlled by the light intensity. In a light gradient, the hematite component directs to the low intensity, exerting a torque on the composite particle. The swimmer reorients and migrates towards the high intensity of the light (Fig. 2B and SI). We use a custom optical setup combining light sources to deliver spatio-temporal patterns with a few microns resolution and 0.01s accuracy and guide the self-assembly (SI).

A dilute suspension of the swimmers is fed to a capillary, residing near the bottom surface at surface density $\Phi_s \sim 10^{-3} \text{ part}/\mu\text{m}^2$. They travel isotropically in uniform light but gather and collide as we superimpose the bright spot of a focused laser ($\lambda = 404 \text{ nm}$), assembling into a self-spinning microgear. The structure is composed of a core vertical swimmer surrounded by 6 peripheral close-packed particles (Fig.1B). The rotor remains stable in uniform light after extinction of the laser spot and its lifetime is set by the duration of the experiment ($\sim 10 - 20 \text{ mins}$). We repeat the light sequence to form rotors. The handedness is random and we measure 49.85% clockwise and 50.15% counter-clockwise from 1017 rotors. The formation is specific and high yield as added particles spontaneously detach from the microgears (movie S4). It shows fidelity, forming self-powered microgears in the absence of a template²⁶ and under limited feedback by an external operator, a key feature in self-assembly.

As hematite is partially absorbing at the wavelength of activation, it sets a gradient of light and reaction rate along the illumination axis. The effect is negligible in most situations but becomes significant as a swimmer crosses the brightest region of a laser spot: for a laser shined from below, the hematite is phoretically lifted, and the swimmer flips vertically. It swims downwards against the bottom wall, producing a hydrodynamic pumping^{27,28}. It attracts the neighboring swimmers, already converging to the area by phototaxis. The swimmers collide heads-on with the central

particle, collectively orienting as they pack at the periphery, forming the self-spinning structure (Fig.1D, 2B). In our experimental conditions, we do not observe decomposition of the hydrogen peroxide nor significant optical forces from the light. Shining the laser from the top does not allow the vertical flipping of a swimmer and inhibits the formation of the rotors. Transient rotors can be formed focusing the laser on a sphere deposited on the substrate, however with limited yield and lifetime, which stresses the importance of the hydrodynamic pumping for the cohesion of the structure. The angular speed ω is tuned by the light intensity (Fig.2C), reflecting the translational velocity of the individual swimmers (Fig. 2C) and shows less than 10% variability amongst a population. At low speeds, $\omega < 3$ rad/s, a fluctuation can flip a peripheral swimmer, which induces the collective reorientation of the shell of the microgear and a reversal of the direction of rotation, though the magnitude of the rotation rate is unchanged (Fig.2C-inset). At higher speeds, unidirectional motion persists over the time of the experiment with reduced fluctuations (Fig.2C-inset). In uniform light, the center of mass of the rotors displays a two-dimensional random walk with a diffusion coefficient $D_R = 0.4 \pm 0.1 \mu\text{m}^2/\text{s}$, larger than a passive particle of comparable size (SI). The rotors show slow migration in light gradients, which we harness to build superstructures.

We probe the influence of a rotor on its surrounding using fluorescent tracers (latex, 200 nm, diffusivity D_c), which concentration $\rho(r)$ is extracted by fluorescence microscopy and azimuthal average (Fig.2D-inset). We observe a radial repulsion from the rotor, constituting a sink of hydrogen peroxide, with $c \propto 1/r$. The tracers migrate in the concentration gradient by diffusiophoresis, with velocity $V_{DP} \propto \nabla c = \alpha/r^2$, ($\alpha > 0$ for a repulsive interaction). At steady state, the flux of particles $j = \rho V_{DP} - D_c \nabla_r \rho$ gives a Boltzmann distribution, $\rho \propto e^{-\frac{\alpha}{D_c r}}$, in an effective repulsive potential, in agreement with the experiment for $\alpha = 48 \pm 10 \mu\text{m}^3/\text{s}$ (Fig.2D).

We now discuss the interactions between pairs of rotors. Rotors radially repel each other as previously observed for latex particles. The radial repulsion is isotropic and insensitive to the absolute or relative handedness of the rotors. We confine the rotors using light patterns: a uniform illumina-

tion in the central region solely actuates the rotors while a sharp gradient at the edge confines them. Following, we observe the existence of short-range tangential interaction for $r \sim 2.0R - 3.0R$, where r is the center-to-center distance of rotors of radii $R \sim 3 \mu\text{m}$. Co-rotating pairs revolve around each other at $\Omega \sim 0.05 \text{ rad/s}$, in the direction of their spin (movie S5, Fig.3A) but do not synchronize (Fig.3B). Counter-rotating pairs are static (Fig.3A, movie S6) and phase-lock at $\pi/6$ as visible from the peak in the Probability Density Function (PDF) of the phase lag $\Psi = |\theta_1| - |\theta_2|$ (Fig.3B). The PDF broadens as the rotors are further apart and becomes asymmetric for pairs with different angular speeds (Fig.3B-inset). This behavior is reminiscent of mechanical cogwheels, in the absence of any contact between the rotors. We rule out hydrodynamics as the main contribution to the tangential interaction, as a torque-free rotor generates a slip-flow opposite to its spin, which makes a co-rotating pair revolve along the common direction of spin, in contrast with the experiment. Besides, the confinement of the pairs hinders the hydrodynamic translation of contra-rotating rotors²⁹.

In order to gain insight into the diffusiophoretic coupling, we study the concentration field surrounding a rotor and simulate the diffusion equation for a structure of 7 impermeable and passive spheres, decorated by 6 chemically active sites (see SI for details). It constitutes a sink of fuel, whose near-field concentration profile presents the 6-fold symmetry of the rotor (Fig.3C). We compute, from the simulated concentration field, the radial, respectively azimuthal, phoretic velocities for a point particle $\tilde{v}_{r,\theta} \propto \nabla_{r,\theta} c(r, \theta)$ and obtain $1/r^2$ decay, respectively $1/r^8$, with $(\tilde{v}_\theta/\tilde{v}_r) \cdot (r/R)^6 \sim 1$ (Fig.3D). The short-range of the tangential interaction originates from the rapid decay of the azimuthal component. It arises from the superimposition of the monopolar concentration field generated by each active site and reflects the azimuthal dependence of the concentration surrounding a sphere with hexapolar chemical activity: $c(r, \theta) \propto P_6(\cos \theta)/r^7$, where P_6 is the Legendre polynomial of 6th degree³⁰. The result is qualitatively unchanged for a bead of finite size (Fig. 3D), which velocity is obtained by integration of the slip on the surface¹², or by

addition of an impermeable wall delineating a semi-infinite space (see SI).

As a result of the fast diffusion of the fuel, $D_{\text{H}_2\text{O}_2} \sim 10^3 \mu\text{m}^2/\text{s}$, the Péclet number of the rotation is low, $\text{Pe} = R^2\omega/D_{\text{H}_2\text{O}_2} \sim 0.01$, and the concentration field is steady in the rotating frame of the rotor. Neighboring rotors interact through the modulation of the concentration field computed above, mirroring the effective energy landscape $U(r, \theta) \propto c(r, \theta)^{20}$. The tangential interaction is short-range and we assume that the azimuthal coupling is set at distance $r - R$, separating the edge of a rotor to the center to its neighbor. The phases θ_i ($i=1,2$) of the rotors in a pair, at fixed distance r , are described by coupled Langevin equations $d\theta_i/dt = \omega_i + \varepsilon Q(\theta_i, \theta_j) + \sqrt{2D_\theta}\zeta(t)$, where i, j identifies the rotor, ω_i their angular speed, εQ is the phoretic coupling between the rotors and $\zeta(t)$ a delta-correlated noise of amplitude D_θ . We independently estimate the amplitude of the phoretic coupling from the radial repulsion, $\varepsilon = \frac{\alpha}{R^3} \cdot \left(\frac{R}{r-R}\right)^8 \sim 2\left(\frac{R}{r-R}\right)^8$. Guided by the numerical results, we approximate the coupling term, $Q = \sin(6\Psi)$, with the phase-lag $\Psi = |\theta_1| - |\theta_2|$. We finally obtain by summation:

$$\frac{d\Psi}{dt} = -\delta\omega + 2\varepsilon \sin(6\Psi) + \sqrt{4D_\theta}\zeta(t)$$

where $\delta\omega$ is the relative speed of the rotors (see SI for details). This is a classical Adler equation of synchronization with noise, also seen as the dynamics of an overdamped Brownian particle in a tilted Washboard potential, $\mathcal{V}(\Psi) = \delta\omega\Psi + (\varepsilon/3)\cos(6\Psi)^{31,32}$. In the absence of noise, the phase is trapped in a potential well at high coupling, $3\delta\omega/\varepsilon < 1$, and slides down the corrugated energy landscape at low coupling³³. This qualitatively describes the phase-locking observed for contra-rotating rotors, for which $\delta\omega \sim 0$, and the slow revolution at Ω of co-rotating pairs, for which $\delta\omega \sim 2\omega$. In the presence of noise, the PDF for Ψ follows a Fokker-Planck equation, which stationary solution is: $P(\Psi) = (1/A)e^{-\mathcal{V}(\Psi)/2D_\theta} \int_{\Psi}^{\Psi+\pi/3} e^{\mathcal{V}(\Psi')/2D_\theta} d\Psi'$, where A is the normalization constant (see SI for details). It shows an excellent agreement with our experimental measurements of the PDF for the phase lag (Fig.3B), with the phoretic coupling ε as single fit parameter, as we independently extract the rotation speeds and noise amplitude, $D_\theta = 0.03 \pm 0.01 \text{ rad}^2/\text{s}$ from individual

tracking of the rotation of the rotors (see SI). The model remarkably captures the asymmetric PDF observed for pairs of contra-rotating rotors with notable speed difference, up to $\Delta\omega/\omega \sim 20\%$, without additional parameters (Fig.3B-inset). The coupling parameter ε decays with increasing distance and shows a good agreement with our prediction, $\varepsilon \sim 2\left(\frac{R}{r-R}\right)^8$, obtained from the radial repulsion between rotors, without adjustable parameters (Fig.3E). For co-rotating pairs, guided by the persistence of the phase lag, we neglect the noise and the difference of rotation speed of the rotors, and obtain $d\theta/dt = \omega + \varepsilon \sin(12\theta)$, predicting a reduced rotation rate $\omega\sqrt{1 - (\varepsilon/\omega)^2}$ (see SI). The short-range of the tangential interaction confines the slowing down to the nearest parts of rotors, effectively acting as partial friction. It qualitatively agrees with the experiment and rotors revolve in the direction of their spin, with $\tilde{\Omega} \sim \omega - \omega\sqrt{1 - (\varepsilon/\omega)^2} \sim \frac{\varepsilon^2}{2\omega} \sim 0.005$ rad/s.

Following our understanding of the pair interaction, we architect machineries, whose collective dynamics arise from microgears with individually selected spins. First, we control the travel speed Ω of the edge-current in hexagonal patterns of 7 co-rotating gears (Fig.1C, 4A), increasing the azimuthal coupling ε through confinement (Fig.4A-inset). Next, we form higher-order assemblies by combination of superstructures: we initiate two contra-rotating sets of 3 co-rotating rotors, each collectively rotating along their common direction of spin (Fig.4B). They are subsequently combined to constitute the synchronized gears of a micromachine (movie S7, Fig.4C), stressing the robustness and versatility of our findings.

Colloidal spinners provide a platform to explore active spinning matter and test theoretical predictions³⁴⁻³⁹, though the competition in our system of long-range diffusiophoretic interactions with hydrodynamics may significantly enrich the dynamics. The interplay between phase synchronization and spatial organization has the potential to achieve new form of self-organization, without equilibrium counterparts nor observed for collections of *translational* self-propelled particles⁴⁰. Our bottom-up approach shows a desirable level of accuracy toward the targeted structure. Com-

binning non-equilibrium interactions with spatiotemporal light sequences, we program dynamical superstructures that autonomously regulate. It makes us architect of Matter and emulates the biological organization into the material world.

References

1. Whitesides, G. M. & Grzybowski, B. Self-assembly at all scales. *Science* **295**, 2418–2421 (2002).
2. Erb, R. M., Son, H. S., Samanta, B., Rotello, V. M. & Yellen, B. B. Magnetic assembly of colloidal superstructures with multipole symmetry. *Nature* **457**, 999–1002 (2009).
3. Sacanna, S., Irvine, W. T. M., Chaikin, P. M. & Pine, D. J. Lock and key colloids. *Nature* **464**, 575–578 (2010).
4. Chen, Q., Bae, S. C. & Granick, S. Directed self-assembly of a colloidal kagome lattice. *Nature* **469**, 381–384 (2011).
5. Wang, Y., Wang, Y., Breed, D., Manoharan, V.N. Feng, L., Hollingsworth, A.D., Weck, M., Pine, D.J., Colloids with valence and specific directional bonding. *Nature* **490**, 51–55 (2012).
6. Damasceno, P. F., Engel, M. & Glotzer, S. C. Predictive Self-Assembly of Polyhedra into Complex Structures. *Science* **337**, 453–457 (2012).
7. Manoharan, V. N. Colloidal matter: Packing, geometry, and entropy. *Science* **349**, 942 (2015).
8. Ducrot, É., He, M., Yi, G.-R. & Pine, D. J. Colloidal alloys with preassembled clusters and spheres. *Nature Materials* **16**, 652–657 (2017).
9. Needleman, D. & Dogic, Z. Active matter at the interface between materials science and cell biology. *Nature Reviews Materials* **2**, 17048–14 (2017).

10. Dey, K. K., Wong, F., Altemose, A. & Sen, A. Catalytic Motors-Quo Vadimus. *Current Opinion in Colloid & Interface Science* **21**, 4–13 (2016).
11. Aubret, A., Ramananarivo, S. & Palacci, J. Eppure si muove, and yet it moves: Patchy (phoretic) swimmers. *Current Opinion in Colloid & Interface Science* **30**, 81–89 (2017).
12. Anderson, J. L. Colloid Transport by Interfacial Forces. *Annual Review Of Fluid Mechanics* **21**, 61–99 (1989).
13. Ramaswamy, S. The Mechanics and Statistics of Active Matter. *Annual Review of Condensed Matter Physics, Vol I* **1**, 323–345 (2010).
14. Cates, M. E., Marenduzzo, D., Pagonabarraga, I. & Tailleur, J. Arrested phase separation in reproducing bacteria creates a generic route to pattern formation. *Proceedings of the National Academy of Sciences of the U.S.A* **107**, 11715–11720 (2010).
15. Bricard, A., Caussin, J.-B., Desreumaux, N., Dauchot, O. & Bartolo, D. Emergence of macroscopic directed motion in populations of motile colloids. *Nature* **503**, 95–98 (2014).
16. Vicsek, T., Czirok, A., Benjacob, E., Cohen, I. & Shochet, O. Novel Type of Phase-Transition in a System of Self-Driven Particles. *Physical Review Letters* **75**, 1226–1229 (1995).
17. Wu, K.-T., Hishamunda, J. B., Chen, D.T. N., DeCamp, S.J., Chang, Y.-W., Fernandez-Nieves, A., Fraden, S., Dogic, Z., Transition from turbulent to coherent flows in confined three-dimensional active fluids. *Science* **355**, eaal1979 (2017).
18. Lushi, E., Wioland, H. & Goldstein, R. E. Fluid flows created by swimming bacteria drive self-organization in confined suspensions. *Proceedings of the National Academy of Sciences of the U.S.A* **111**, 9733–9738 (2014).

19. Wang, W., Duan, W., Sen, A. & Mallouk, T. E. Catalytically powered dynamic assembly of rod-shaped nanomotors and passive tracer particles. *Proceedings Of The National Academy Of Sciences Of The United States Of America* **110**, 17744–17749 (2013).
20. Banerjee, A., Williams, I., Azevedo, R. N., Helgeson, M. E. & Squires, T. M. Solutio-inertial phenomena: Designing long-range, long-lasting, surface-specific interactions in suspensions. *Proceedings of the National Academy of Sciences of the U.S.A* **113**, 8612–8617 (2016).
21. Shields IV, C. W. & Velev, O. D. The Evolution of Active Particles: Toward Externally Powered Self-Propelling and Self-Reconfiguring Particle Systems. *CHEMPR* **3**, 539–559 (2017).
22. Vutukuri, H. R., Bet, B., Roij, R. x., Dijkstra, M. & Huck, W. T. S. Rational design and dynamics of self-propelled colloidal bead chains: from rotators to flagella. *Scientific Reports* **7** 1–14 (2017).
23. Palacci, J., Sacanna, S., Steinberg, A. P., Pine, D. J. & Chaikin, P. M. Living Crystals of Light-Activated Colloidal Surfers. *Science* **339**, 936–940 (2013).
24. Youssef, M., Hueckel, T., Yi, G.-R. & Sacanna, S. Shape-shifting colloids via stimulated dewetting. *Nature Communications* **7**, 1–7 (2016).
25. Howse, J. R., Richard A.L., Ryan, A.J., Gough, T., Vafabakhsh, R., Golestanian, R. Self-motile colloidal particles: From directed propulsion to random walk. *Physical Review Letters* **99**, 048102–5 (2007).
26. Maggi, C., Simmchen, J., Saglimbeni, F., Katuri, J., Dipalo, M., De Angelis, F., Sanchez, S., Di Leonardo, R., Self-Assembly of Micromachining Systems Powered by Janus Micromotors. *Small* **12**, 446–451 (2015).
27. Weinert, F. M. & Braun, D. Observation of Slip Flow in Thermophoresis. *Physical Review Letters* **101**, 168301–4 (2008).

28. Di Leonardo, R., Ianni, F. & Ruocco, G. Colloidal Attraction Induced by a Temperature Gradient. *Langmuir* **25**, 4247–4250 (2009).
29. Leoni, M. & Liverpool, T. B. Dynamics and interactions of active rotors. *Europhysics Letters* **92**, 64004–7 (2011).
30. Golestanian, R., Liverpool, T. B. & Ajdari, A. Designing phoretic micro- and nano-swimmers. *New Journal of Physics* **9**, 126-135 (2007).
31. Adler, R. Locking Phenomena in Oscillators. *Proceedings of the IEEE* **61**, 1380–1385 (1973).
32. Di Leonardo, R., Búzás, A., Kelemen, L., Vizsnyiczai, G., Oroszi, L. & Ormos, P. Hydrodynamic Synchronization of Light Driven Microrotors. *Physical Review Letters* **109**, 034104 (2012).
33. Shlomovitz, R., Roongthumskul, Y., Ji, S., Bozovic, D. & Bruinsma, R. Phase-locked spiking of inner ear hair cells and the driven noisy Adler equation. *Interface Focus* **4**, 20140022–20140022 (2014).
34. Spellings, M., Engel, M., Klotsa, D., Sabrina, S., Drews, A., M and Nguyen, N. H. P., Bishop, K.J.M., Glotzer, S.C. Shape control and compartmentalization in active colloidal cells. *Proceedings Of The National Academy Of Sciences Of The United States Of America* **112**, E4642–E4650 (2015).
35. Yeo, K., Lushi, E. & Vlahovska, P. M. Collective Dynamics in a Binary Mixture of Hydrodynamically Coupled Microrotors. *Physical Review Letters* **114**, 188301–5 (2015).
36. Uchida, N. & Golestanian, R. Generic Conditions for Hydrodynamic Synchronization. *Physical Review Letters* **106**, 058104–4 (2011).

37. Nguyen, N. H. P., Klotsa, D., Engel, M. & Glotzer, S. C. Emergent Collective Phenomena in a Mixture of Hard Shapes through Active Rotation. *Physical Review Letters* **112**, 075701–5 (2014).
38. Guzman-Lastra, F., Kaiser, A. & Loewen, H. Fission and fusion scenarios for magnetic microswimmer clusters. *Nature Communications* **7**, 13519–10 (2016).
39. Fily, Y., Baskaran, A. & Marchetti, M. C. Cooperative self-propulsion of active and passive rotors. *Soft Matter* **8**, 3002–8 (2012).
40. van Zuiden, B. C., Paulose, J., Irvine, W. T. M., Bartolo, D. & Vitelli, V. Spatiotemporal order and emergent edge currents in active spinner materials. *Proceedings Of The National Academy Of Sciences Of The United States Of America* **113**, 12919–12924 (2016).

Supplementary Information is available in the online version of the paper

Acknowledgements We thank L. Bocquet and P. Chaikin for enlightening discussions. This material is based upon work supported by the National Science Foundation under Grant No. DMR-1554724. J.P. thanks the Sloan Foundation for support through grant FG-2017-9392. S.S. acknowledges support from the NSF CAREER award DMR-1653465.

Authors Contribution M.Y. and S.S. conceived and synthesized the colloidal particles. A. A. performed the experiment and analyzed the experimental results. A.A. and J.P. conceived the project, designed the experiment, worked out the model and wrote the manuscript.

Competing Interests The authors declare that they have no competing financial interests.

Correspondence Correspondence and requests for materials should be addressed to J.P. (email: palacci@ucsd.edu).

Data Availability Statement The data that support the plots within this paper and other findings of this study are available from the corresponding author upon request.

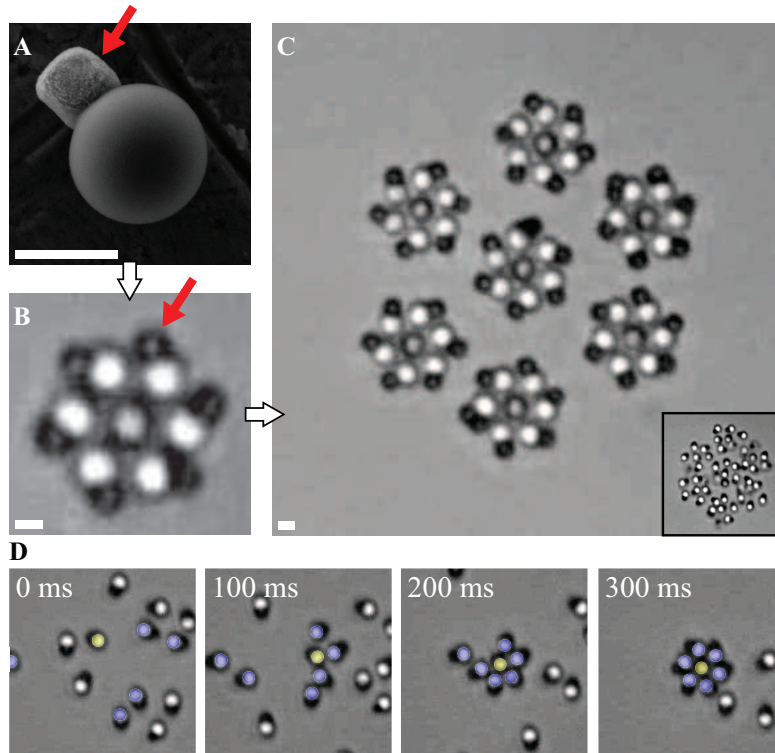


Figure 1: Hierarchical Self-Assembly of Self-Spinning Rotors. A) Scanning Electron Microscopy (SEM) of the phototactic swimmer with a fore-aft asymmetry and consisting of the extrusion of the hematite cube from a chemically inert polymer bead. The particles self-propel in hydrogen peroxide fuel under light activation, with the bead heading. B) Bright-Field (BF) picture of a self-spinning rotor self-assembled from 7 phototactic swimmers. The core-particle is flipped vertically and surrounded by 6 peripheral swimmers, which orientation defines the spinning direction. The handedness of the rotor is random, clockwise and counterclockwise rotors are equiprobable. C) BF imaging of a dynamical superstructure obtained first by the sequential formation of rotors, then confined thanks to controlled spatiotemporal light patterns. C-inset) The self-assembly is purely dissipative, switching off the light, the system returns to equilibrium and the order is destroyed by thermal noise. D) Timelapse of the rapid self-assembly of phototactic swimmers into self-spinning microgear triggered by a focused laser beam. A particle crosses the high intensity of a laser beam and flips vertically, swimming downwards (yellow particle). It generates a pumping flow that attracts the peripheral (blue) particles and forms a rotor (see main text). Scale bars are $1 \mu\text{m}$, red arrows indicate the photoactive hematite part.

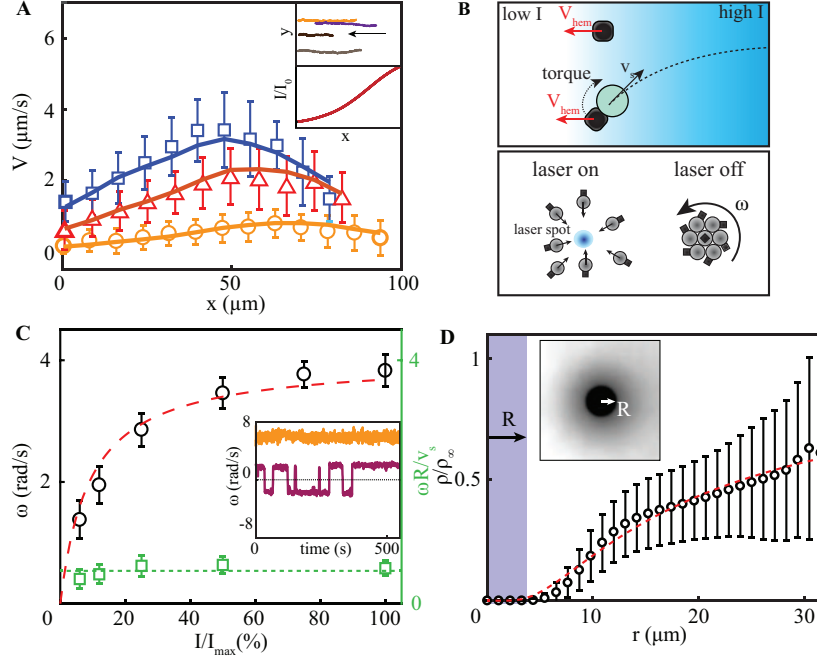


Figure 2: Light-guided Assembly A) Migration speed of hematite cubes (empty symbols) in different light gradients (colors) and comparison with the diffusiophoretic propulsion $V \propto \nabla c \propto \nabla \nu(I)$ (solid lines) obtained from the independent measurement of the intensity profile and a single fit parameter (see Main Text). A-inset) Example of particles trajectories (top) and light profile (bottom). Hematite migrates towards the low intensity of light (black arrow). B) Sketch of the phototactic mechanism (top) and microgears assembly (bottom). The hematite exerts a torque on the composite swimmers, which travel toward the high intensity (top). They direct toward the bright spot of a focused laser (blue spot). The central swimmer flips, inducing an attractive hydrodynamic, that assemble the neighboring swimmers into a spinning microgear (bottom) [See main text]. C) The microgears rotate at ω , tuned by the intensity of the light (left axis, black circles) reflecting the translational velocity V_s of the phototactic swimmers (red dashed line). The ratio $\omega R/V_s$ is constant (right axis, green squares). B-Inset) Time evolution of the rotation rate ω for rotors at different speeds. At low speed, $\omega \sim 2$ rad/s, fluctuations flip the direction of rotation at constant magnitude $|\omega|$ (violet curve). At higher speeds, the rotation is persistent at constant $\omega = 5.9 \pm 0.4$ rad/s (orange curve). D) Normalized fluorescence showing the repulsion of 200nm fluorescent beads by a rotor. The density ρ of the beads is azimuthally and temporally averaged from the fluorescence imaging (D-inset) and described by a phoretic repulsion in the gradient of fuel induced by the presence of the rotor: $\rho \propto \exp(-\alpha/rD_c)$ with $\alpha = 48 \pm 10 \mu\text{m}^3/\text{s}$ (red dashed line). Error bars are one standard deviation.

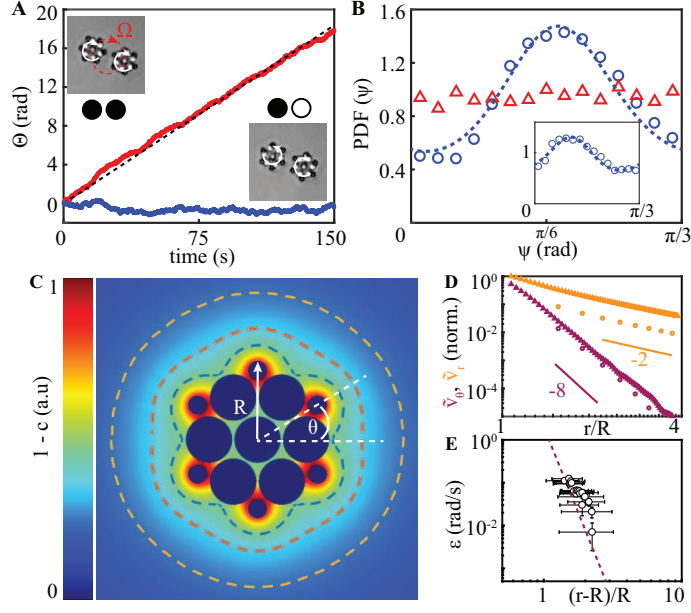


Figure 3: Rotors Pair-Interactions. A) Co-rotating pairs revolve at $\Omega \sim 0.1$ rad/s along the common spin (red curve), counter-rotating pairs are static (blue curve). B) Probability Distribution Function (PDF) of the phase difference Ψ between the rotors. The PDF is flat for co-rotating pairs (red triangles) and shows a peak of synchronization at $\pi/6$ for counter-rotating pairs (blue circles). It is described by a Langevin model of chemically coupled oscillators (dashed line) with the phoretic coupling ε as single fit parameter (see Main text). B-inset) Contra-rotating pairs, with different rotation speeds, exhibit an asymmetric PDF(Ψ) with a shifted maximum (blue circles), a behavior remarkably captured by the model (dashed line). C) Simulated concentration of fuel c surrounding a rotor modeled as a structure of 7 impermeable and passive spheres, decorated by 6 chemically-active sites (SI for numerical details). Dashed lines are isocontours. The concentration field exhibits the 6-fold symmetry of the rotor in the near-field and is isotropic further. It induces the short-range directional interactions between rotors. D) Radial, $\tilde{v}_r \propto 1/r^2$ (orange symbols), and azimuthal, $\tilde{v}_\theta \propto 1/r^8$ (violet symbols), diffusiophoretic velocities obtained from the simulated concentration field for a point-particle (triangles) and a bead of finite radius $0.3R$ (circles). E) Phoretic coupling ε obtained by fit of the PDF(Ψ) (Fig.3B) for contra-rotating pairs (black symbols), and comparison with the prediction $\varepsilon \sim 2\left(\frac{R}{r-R}\right)^8$ obtained from the radial repulsion, without adjustable parameters (violet dashed line, see Main Text). Error bars: standard deviation for the distance and standard deviation for the parameter ε obtained by bootstrap method, fitting 500 synthetic data sets for each point in the graph.

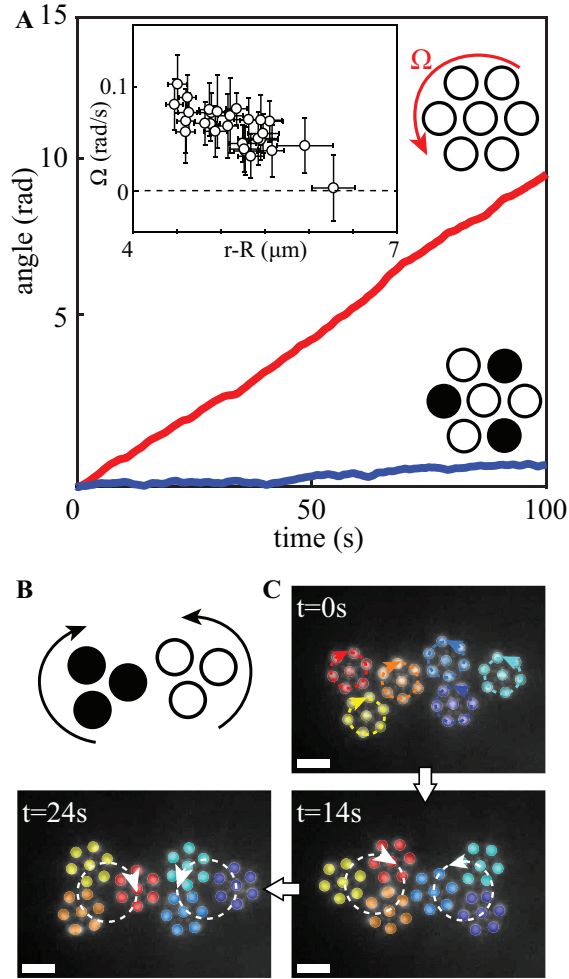


Figure 4: Dynamical Superstructures. A) Collections of 7 rotors form a hexagonal arrangement as a result of radial repulsion and confinement. The dynamics is set by the interplay between spins and spatial coordinates of the components: co-rotating gears exhibit edge current traveling at $\Omega \sim 0.1$ rad/s along the common direction of spin (red curve), gears with alternating spins are static (blue curve). A-inset) The amplitude of Ω is controlled by the confinement of the structure as the azimuthal coupling ε decreases with distance (see Main Text). Error bars are one standard deviation. B) Superstructure made of 2 sets of 3 co-rotating gears, with opposite spins. C) Hierarchical assembly of those two sets into a structure, leads to a synchronous motion of the two sets as visible on the time-lapse pictures. The false colors show the time evolution of the rotors in each set. Black, respectively white, disks represent clockwise, respectively counter-clockwise, rotors.